

Chemical Abundances of the Secondary Star in the Black Hole X-Ray Binary V404 Cygni

Jonay I. González Hernández^{1,2}, Jorge Casares^{1,2}, Rafael Rebolo^{1,2,3}, Garik Israelian^{1,2},
Alexei V. Filippenko⁴, and Ryan Chornock^{4,5}

ABSTRACT

We present a chemical abundance analysis of the secondary star in the black hole binary V404 Cygni, using Keck I/HIRES spectra. We adopt a χ^2 -minimization procedure to derive the stellar parameters, taking into account any possible veiling from the accretion disk. With these parameters we determine the atmospheric abundances of O, Na, Mg, Al, Si, Ca, Ti, Fe, and Ni. The abundances of Al, Si, and Ti appear to be slightly enhanced when comparing with average values in thin-disk solar-type stars. The O abundance, derived from optical lines, is particularly enhanced in the atmosphere of the secondary star in V404 Cygni. This, together with the peculiar velocity of this system as compared with the Galactic velocity dispersion of thin-disk stars, suggests that the black hole formed in a supernova or hypernova explosion. We explore different supernova/hypernova models having various geometries to study possible contamination of nucleosynthetic products in the chemical abundance pattern of the secondary star. We find reasonable agreement between the observed abundances and the model predictions. However, the O abundance seems to be too high regardless of the choice of explosion energy or mass cut, when trying to fit other element abundances. Moreover, Mg appears to be underabundant for all explosion models, which produces Mg abundances roughly 2 times higher than the observed value.

Subject headings: black holes: physics — stars: abundances — stars: evolution — stars: individual V404 Cygni (=GS 2023+338) — supernovae: general — X-rays: binaries

1. Introduction

The low-mass X-ray binary (LMXB) V404 Cygni is one of the most compelling cases for a black hole accreting mass from a low-mass companion (secondary star). The mass function is among the highest values in such binary systems ($f(M) = 6.08 \pm 0.06 M_{\odot}$; Casares et al. 1992;

Casares & Charles 1994), placing the mass of the compact object comfortably above the upper limit of a rapidly rotating neutron star. The mass ratio of the system, $q = M_2/M_{\text{BH}} = 0.060^{+0.004}_{-0.005}$, was derived from the measurement of the rotation velocity of the secondary star, $v \sin i = 39.1 \pm 1.2 \text{ km s}^{-1}$ (Casares & Charles 1994).

Shahbaz et al. (1994) modelled the ellipsoidal variations using a K -band infrared (IR) light curve of V404 Cygni and derived an orbital inclination of $i = 56^\circ \pm 4^\circ$, and consequently the implied mass of the black hole is $M_{\text{BH}} = 12 \pm 2 M_{\odot}$. Later, Pavlenko et al. (1996) studied the R -band light curve to determine an inclination of $i = 56^\circ \pm 2^\circ$. More recently, Khargharia et al. (2010) derived a K3 III spectral type for the secondary star from near-IR (NIR) spectroscopy of V404 Cygni, and Sanwal et al. (1996) remodeled the H -band light

¹Instituto de Astrofísica de Canarias (IAC), E-38205 La Laguna, Tenerife, Spain; jonay@iac.es, jcv@iac.es, rrl@iac.es, gil@iac.es

²Depto. Astrofísica, Universidad de La Laguna (ULL), E-38206 La Laguna, Tenerife, Spain

³Consejo Superior de Investigaciones Científicas, Spain

⁴Department of Astronomy, University of California, Berkeley, CA 94720-3411, USA; alex@astro.berkeley.edu

⁵Harvard-Smithsonian Center for Astrophysics, 60 Garden Street, Cambridge, MA 02138, USA; rchornock@cfa.harvard.edu

curve; they refined the orbital inclination to be $i = (67_{-1}^{+3})^\circ$, which yields a black hole mass of $M_{\text{BH}} = 9_{-0.6}^{+0.2} M_\odot$.

The system is placed near the Galactic plane, with a Galactic latitude of $b \approx -2.1^\circ$. Miller-Jones et al. (2009b) recently derived the distance with very long baseline interferometry (VLBI) observations, $d = 2.39 \pm 0.14$ kpc. They revisited the analysis of Miller-Jones et al. (2009a) to determine a more accurate peculiar velocity of 39.9 ± 5.5 km s⁻¹. This value is significantly lower than their previous one, $v_{\text{pec}} \sim 64$ km s⁻¹ (Miller-Jones et al. 2009a) assuming a distance of 4 kpc (Jonker & Nelemans 2004), and it can be achieved via a Blaauw (1961) velocity kick; thus, no asymmetric supernova kick is required. However, Miller-Jones et al. (2009b) argued that the component of the peculiar velocity in the Galactic plane, 39.6 km s⁻¹, is still too large to come from the intrinsic velocity dispersion of the Galactic plane, which is 18.9 km s⁻¹ (Mignard 2000) for the likely F0–F5 progenitor of the donor star. Thus, this peculiar velocity should come from a natal kick from the ejection of material in a supernova (SN) or a more energetic hypernova (HN) event, but its magnitude does not require an additional asymmetric kick.

The chemical abundances of secondary stars in black hole and neutron star X-ray binaries have been studied for several systems: Nova Scorpii 1994 (Israelian et al. 1999; González Hernández et al. 2008a), A0620–00 (González Hernández et al. 2004), Centaurus X-4 (González Hernández et al. 2005), XTE J1118+480 (González Hernández et al. 2006; González Hernández et al. 2008b), and V4641 Sagittarii (Orosz et al. 2001; Sadakane et al. 2006). The metallicities of these binary systems are all close to solar independent of their location with respect to the Galactic plane. In addition, the above authors have taken into account different scenarios of SN/HN ejecta pollution on the photospheric abundances of the secondary star.

In this paper, we use high-resolution spectra to derive the stellar parameters and chemical abundances of the secondary star in the black hole X-ray binary V404 Cygni. We then compare in detail these element abundances in the context of the possible enrichment of the secondary star from SN/HN yields.

2. Observations

We obtained 14 high-quality spectra of V404 Cygni in quiescence with the High Resolution Spectrometer (HIRES; Vogt et al. 1994) at the Keck I 10-m telescope (Mauna Kea, Hawaii) on 12 July 2009 UT. The data covered the spectral regions 4390–5805 Å, 5895–7405 Å, and 7520–8780 Å with a slit width of $0.861''$, at a resolving power $\lambda/\Delta\lambda \approx 50,000$. The seeing was in the range $0.6''$ – $1.0''$ during the whole night, and for most of the main target spectra it was $\sim 0.75''$. This observing program was scheduled at a time such that the secondary star was near inferior conjunction with the black hole (i.e., at an orbital phase of 0), to minimize possible effects on the determination of chemical abundances due to the asymmetry of its Roche lobe.

We also observed ten template stars with spectral types in the range K0V/IV–K2V with the same instrument and spectral configuration. The integration time for V404 Cygni was fixed at 1800 s in all exposures except for the last two, which were of 2100 s and 2000 s duration. This relatively long integration time was chosen because the orbital smearing at this phase is only 3 – 5 km s⁻¹, smaller than the instrumental resolution of ~ 6.6 km s⁻¹.

The spectra were reduced in a standard manner using the MAKEE package. Each order of each individual spectrum was normalized using a low-order cubic spline and combined into a single one-dimensional spectrum. The individual spectra were corrected for their radial velocity (for more details, see González Hernández et al. 2011, in preparation) and combined in order to improve the signal-to-noise ratio (S/N). After binning in wavelength in steps of 0.1 Å, the final spectrum had $S/N \approx 70$ in the continuum at 6500 Å and $S/N \approx 150$ at 7770 Å. This spectrum is displayed in Figure 1, in comparison with that of a K2 V template star. Note that the spectrum of the secondary star in this system and the spectra of the template stars were normalized using the same procedure.

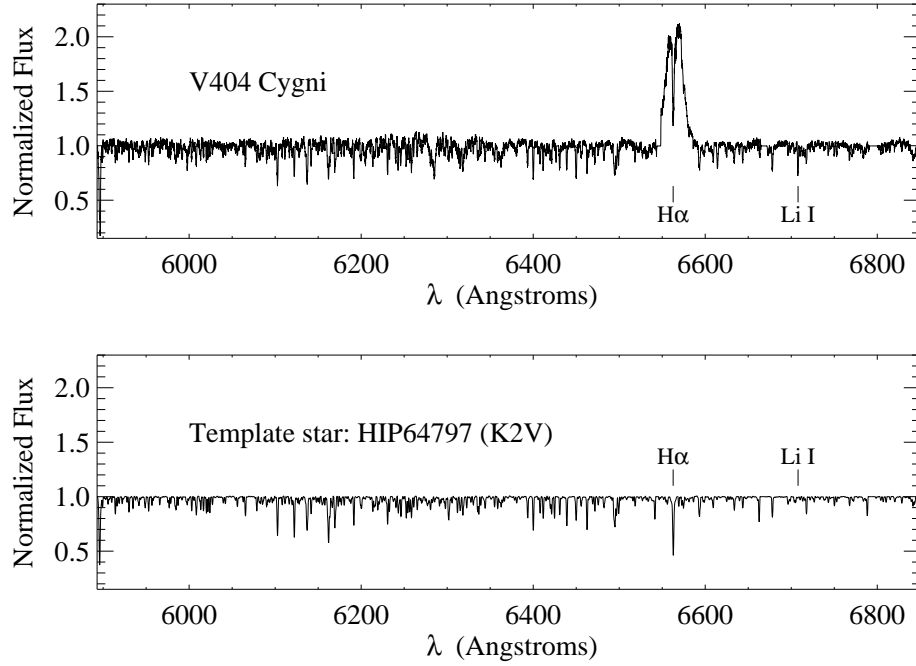


Fig. 1.— Observed spectrum of the secondary star of V404 Cygni, after correcting for the individual radial velocities and combining all individual spectra (top panel), and a properly broadened template also corrected for its radial velocity (HIP 64797, bottom panel).

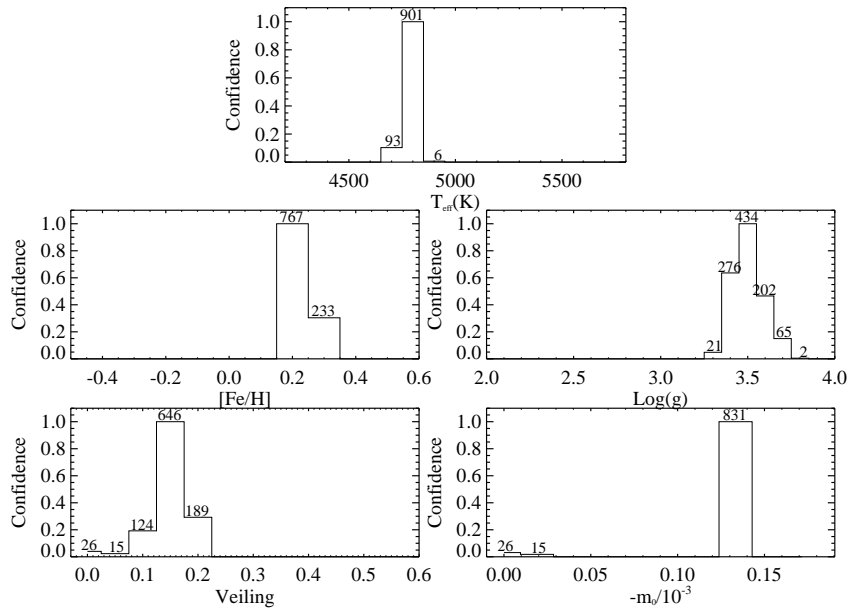


Fig. 2.— Distributions obtained for each parameter using Monte Carlo simulations. The bottom-right panel shows the distribution obtained for the veiling slope, m_0 , given as $-m_0/10^{-3}$ in units of \AA^{-1} . The labels at the top of each bin indicate the number of simulations consistent with the bin value. The total number of simulations was 1000.

TABLE 1
RANGES AND STEPS OF MODEL PARAMETERS

Parameter	Range	Step
T_{eff}	4200 \rightarrow 5800 K	100 K
$\log[g/(\text{cm s}^2)]$	2 \rightarrow 4	0.1
[Fe/H]	-0.5 \rightarrow 0.6	0.1
f_{4500}	0 \rightarrow 0.6	0.05
m_0	0 \rightarrow -0.000171	-0.000019

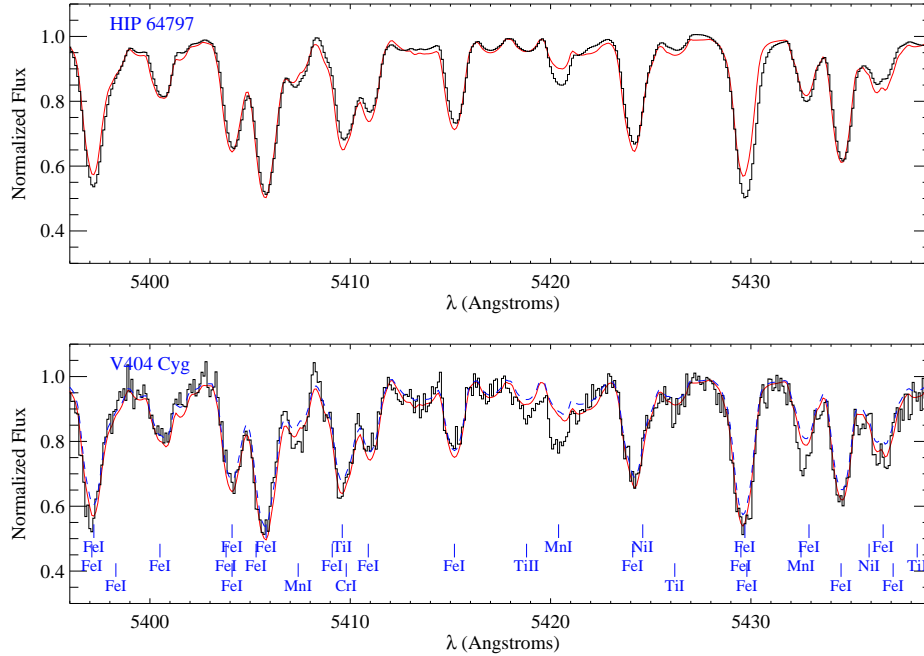


Fig. 3.— Best synthetic spectral fits to the Keck/HIRES spectrum of the secondary star in the V404 Cygni system (bottom panel), and the same for a template star (properly broadened) shown for comparison (top panel). Synthetic spectra are computed for solar abundances (dashed line) and best-fit abundances (solid line).

3. Chemical Analysis

3.1. Stellar Parameters

The merged and normalized spectrum of the secondary star in V404 Cygni may show apparently weaker stellar lines due to the veiling introduced by the accretion disk. This veiling is found to be $\sim 13\% \pm 2\%$ in the range 6400–6600 Å in a set of observations taken during the period 1990–1993 (Casares & Charles 1994). This veiling was estimated by performing standard optimal subtraction techniques with a K0 IV template star.

The high quality and resolution of the Keck/HIRES spectrum enable us to infer the stellar param-

eters, (T_{eff} , $\log g$, and the metallicity [Fe/H]) of the companion star, taking into account any possible veiling from the accretion disk as in previous studies of other LMXBs (see, e.g., González Hernández et al. 2004; González Hernández et al. 2008b). For simplicity, the veiling was defined as a linear function of wavelength and thus described with two additional parameters, the veiling at 4500 Å, $f_{4500} = F_{\text{disk}}^{4500} / F_{\text{sec}}^{4500}$, and the slope, m_0 . We note that the total flux is defined as $F_{\text{total}} = F_{\text{disk}} + F_{\text{sec}}$, where F_{disk} and F_{sec} are the flux contributions of the disk and the continuum of the secondary star, respectively.

The most recent version of this code (see

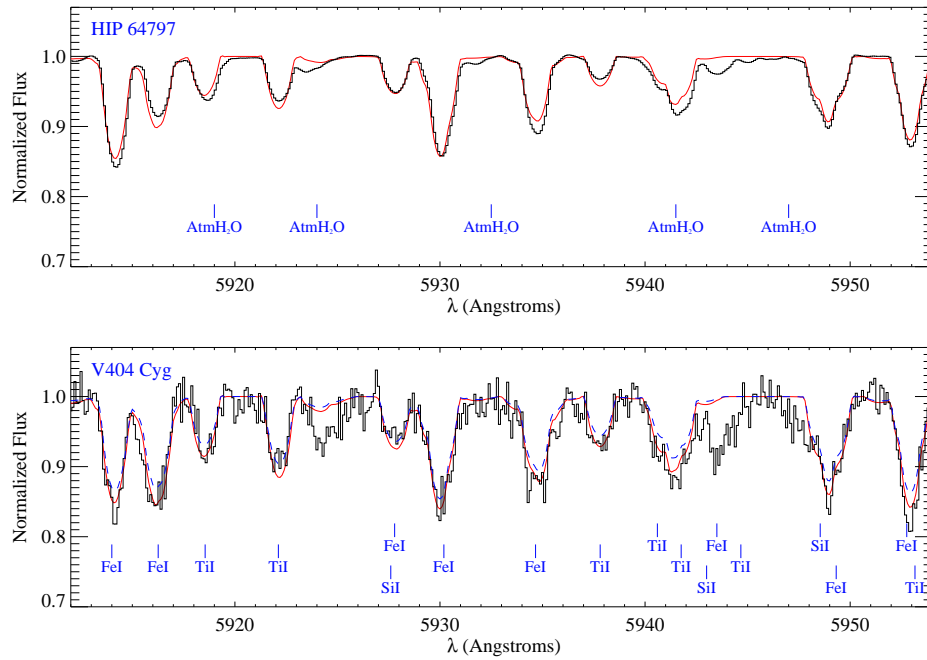


Fig. 4.— The same as in Fig. 3, but for the spectral range 5910–5955 Å. In this spectral region there are several relatively weak telluric lines labelled as AtmH₂O.

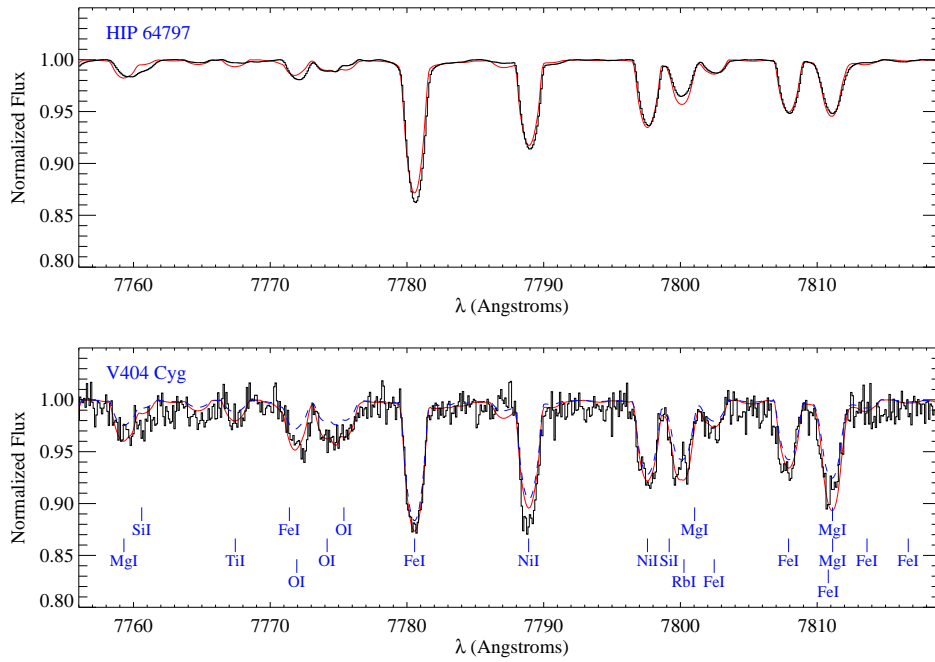


Fig. 5.— The same as in Fig. 3, but for the spectral range 7756–7819 Å.

also González Hernández et al. 2009) allows us to compare, via a χ^2 -minimization procedure, up to 50 small spectral regions of the stellar spectrum with a grid of synthetic spectra computed using the local thermodynamical equilibrium (LTE) code MOOG (Snedden 1973). We used a grid of LTE model atmospheres (Kurucz et al. 1993) and the atomic line data from the Vienna Atomic Line Database (VALD Piskunov et al. 1995). The oscillator strengths of relevant lines were adjusted until they reproduced the solar atlas (Kurucz et al. 1984) with solar abundances (Grevesse et al. 1996). The corrections applied to the $\log gf$ values taken from the VALD database were smaller than ~ 0.2 dex.

We inspected the high-quality HIRES spectrum of V404 Cygni, trying to search for Fe I–Fe II lines. We finally selected 16 spectral features containing more than 50 Fe lines with excitation potentials between 1 and 5 eV. We emphasize that these Fe lines have a range of $\log gf$ values and are spread over the whole spectral range 5100–6750 Å, and we try to find the best-fit model for different veiling factors and various veiling slopes. Therefore, the strength of a given spectral feature depends not only on the stellar parameters and metallicity of the star but also on the veiling factor appropriate for that feature at the corresponding wavelength. In addition, due to the relatively high rotation velocity of the secondary star, these Fe lines were blended with stellar lines of other elements such as Ti and Ni. However, the main contributors to the selected features were always the Fe lines, and the abundances of other elements were in any case scaled with the metallicity of the model.

The five free parameters were varied in the ranges given in Table 1. The rotation velocity of the companion star was measured to be 36.4 km s^{-1} using the HIRES spectrum (for further details, see González Hernández et al. 2011, in preparation), and a limb darkening of $\epsilon = 0.65$ was adopted. The microturbulence, ξ , was computed using an experimental expression as a function of effective temperature and surface gravity (Allende Prieto et al. 2004). The value for the best-fit model given below is $\xi = 1.117 \text{ km s}^{-1}$.

We obtain as most likely values $T_{\text{eff}} = 4800 \pm 100 \text{ K}$, $\log[g/(\text{cm s}^2)] = 3.50 \pm 0.15$, $[\text{Fe}/\text{H}] = 0.20 \pm 0.17$, $f_{4500} = 0.15 \pm 0.05$, and $m_0 = -0.00013 \pm 0.00002$. The 1σ uncertainties of the

five free parameters were determined using 1000 realizations whose corresponding histograms are displayed in Figure 2. Thus, we find a very small veiling, with $f_{5170} \approx 0.05$ for the spectral region of the Mg I b triplet at 5167–5183 Å and almost zero for longer wavelengths. This veiling is lower than that measured during early phases of quiescence (Casares et al. 1993). We emphasize that the linear function adopted to model the behavior of the veiling is strictly valid only in the spectral range 5000–6800 Å, and therefore should not be extrapolated beyond that wavelength range. On the other hand, we have analyzed several spectral ranges around 7750 Å, 8450 Å, and 8750 Å by assuming a veiling $f_{\text{NIR}} = 0$ for all of them, and the Fe I lines in these regions seem to be well reproduced by the spectral synthesis. However, a veiling of 0 throughout the infrared might not be correct, and one would have to analyze spectral lines in the infrared to check if this veiling, derived in the optical, holds for longer wavelengths.

The stellar parameters of secondary stars in LMXBs are particularly relevant for the determination of orbital inclinations, which are typically derived from the modelling of ellipsoidal variations using optical and NIR light curves at quiescence (see, e.g., Gelino et al. 2006). Shahbaz et al. (1994) derived $T_{\text{eff}} \approx 4360 \text{ K}$ for the companion star in their modelling of the *K*-band light curve of V404 Cygni. Hynes et al. (2009) suggest that its most likely spectral is K0 III, which implies $T_{\text{eff}} \approx 4570 \text{ K}$ using the temperature scale of giants in van Belle et al. (1999). Khargharia et al. (2010), however, propose a spectral type of K3 III as the best template that matches their NIR broad-band spectra with little contribution from the accretion disk, providing a veiling of $\sim 2\%$ and $\sim 3\%$ for their *H*– and *K*-band spectroscopy. This spectral type lends to a $T_{\text{eff}} \sim 4300 \text{ K}$, according to their model. However, our spectroscopic value ($T_{\text{eff}} \approx 4800 \text{ K}$) may require more contribution of the flux from the accretion disk in the NIR bands (see, e.g., Hynes et al. 2005), which may also imply a different orbital inclination, and therefore a different black hole mass.

We have collected the most updated information on orbital parameters for several X-ray binaries from the literature to derive the expected size of the Roche lobe and thus the corresponding surface gravity. We compare these values with our

TABLE 2
CHEMICAL ABUNDANCES OF THE SECONDARY STAR IN V404 CYGNI

Element	$\log \epsilon(X)_{\odot}^a$	[X/H]	[X/Fe]	σ	Δ_{σ}	ΔT_{eff}	$\Delta_{\log g}$	Δ_{ξ}	Δ_{vel}	$\Delta[\text{X}/\text{H}]$	$\Delta[\text{X}/\text{Fe}]$	n^b
Fe	7.50	0.23	–	0.12	0.02	0.05	0.00	–0.16	0.08	0.19	–	51
O ^d	8.74	0.60	0.37	0.07	0.05	–0.16	0.06	–0.06	0.06	0.20	0.24	2
Na	6.33	0.30	0.07	0.20	0.12	0.10	–0.03	–0.13	0.10	0.23	0.14	3
Mg	7.58	0.00	–0.23	0.09	0.03	0.06	–0.03	–0.09	0.08	0.15	0.09	8
Al	6.47	0.38	0.15	0.07	0.05	0.05	0.00	–0.08	0.05	0.11	0.11	2
Si	7.55	0.36	0.13	0.22	0.06	–0.06	0.04	–0.10	0.06	0.15	0.15	14
Ca	6.36	0.20	–0.03	0.16	0.05	0.11	–0.04	–0.24	0.10	0.29	0.12	11
Ti	5.02	0.42	0.19	0.24	0.06	0.15	0.02	–0.28	0.12	0.34	0.17	15
Cr	5.67	0.31	0.08	0.15	0.07	0.15	–0.05	–0.07	0.07	0.20	0.16	5
Ni	6.25	0.21	–0.02	0.32	0.11	0.06	–0.00	–0.25	0.14	0.31	0.15	9

NOTE.—Chemical abundances and uncertainties due to the uncertainties $\Delta T_{\text{eff}} = +100$ K, $\Delta_{\log g} = +0.15$ dex, $\Delta_{\xi} = +0.5$ km s^{–1}, and $\Delta_{\text{vel}} = 0.05$.

^aThe solar element abundances were adopted from Grevesse et al. (1996) for all elements except oxygen which was taken from Ecuivillon et al. (2006).

^bThe uncertainties from the dispersion of the best fits to different features, Δ_{σ} , are estimated using the following formula: $\Delta_{\sigma} = \sigma/\sqrt{N}$, where σ is the standard deviation of the measurements.

^cNumber of spectral features of this element analyzed in the star, or if there is only one, its wavelength.

^dThe oxygen abundance has been corrected for NLTE effects, $\Delta_{\text{NLTE}} = -0.2$, using the NLTE computations in Ecuivillon et al. (2006).

TABLE 3
SURFACE GRAVITIES IN LMXBs

Name*	P_{orb} [days]	$M_{\text{CO},f}$ [M_{\odot}]	$M_{2,f}$ [M_{\odot}]	q_f	$a_{c,f}$ [R_{\odot}]	R_L [R_{\odot}]	$\log g(R_L)$	$\log g(\text{spec})$
V404 Cygni	$6.47129 \pm (7 \times 10^{-5})$	9.00 ± 0.60	0.54 ± 0.08	0.060 ± 0.005	30.98 ± 0.75	5.51 ± 0.27	2.69 ± 0.03	3.50 ± 0.15
Cen X-4	$0.6290522 \pm (4 \times 10^{-7})$	1.50 ± 0.40	0.30 ± 0.09	0.200 ± 0.030	3.76 ± 0.38	0.95 ± 0.14	3.96 ± 0.02	3.90 ± 0.30
A0620-00	$0.32301405 \pm (1 \times 10^{-8})$	6.61 ± 0.25	0.40 ± 0.05	0.060 ± 0.004	3.79 ± 0.05	0.67 ± 0.02	4.38 ± 0.02	4.20 ± 0.30
Nova Sco 94	$2.62168 \pm (1.4 \times 10^{-4})$	6.59 ± 0.45	2.76 ± 0.33	0.419 ± 0.028	16.85 ± 0.48	5.17 ± 0.24	3.45 ± 0.01	3.70 ± 0.20
XTE J1118	$0.1699339 \pm (2 \times 10^{-7})$	8.30 ± 0.28	0.22 ± 0.07	0.027 ± 0.009	2.64 ± 0.04	0.37 ± 0.05	4.65 ± 0.04	4.60 ± 0.30

*References: V404 Cygni: Casares & Charles (1994), Casares (1996), Khargharia et al. (2010), and this work; Centaurus X-4: Torres et al. (2002), González Hernández et al. (2005), Casares et al. (2007), Khargharia et al. (2010); A0620-00: González Hernández et al. (2004), Neilsen et al. (2008), González Hernández & Casares (2010), Cantrell et al. (2010); Nova Scorpii 1994: van der Hooft et al. (1998), González Hernández et al. (2008a), Shahbaz (2003); XTE J1118+480: Torres et al. (2004), Gelino et al. (2006), González Hernández et al. (2006), González Hernández et al. (2008b) and this work;

NOTE.—Comparison between LMXB surface gravity determined spectroscopically, $\log g(\text{spec})$, with the surface gravity, $\log g(R_L)$, computed from the orbital period, P_{orb} , the mass ratio, q_f , and the current masses of the compact object, $M_{\text{CO},f}$, and the secondary star, $M_{2,f}$.

TABLE 4
KINEMATICAL PROPERTIES IN LMXBS

Name*	K_2 [km s ⁻¹]	$f(M)$ [M _⊙]	$v \sin i$ [km s ⁻¹]	γ [km s ⁻¹]	d [Kpc]	μ_α [mas yr ⁻¹]	μ_δ [mas yr ⁻¹]
V404 Cygni	208.4 ± 0.6	6.09 ± 0.04	40.8 ± 0.9	0.3 ± 0.6	2.39 ± 0.14	-5.04 ± 0.02	-7.64 ± 0.03
Cen X-4	144.6 ± 0.3	0.197 ± 0.001	44 ± 3	189.6 ± 0.2	1.30 ± 0.40	11 ± 10	-56 ± 10
A0620-00	435.4 ± 0.5	3.10 ± 0.04	82 ± 2	8.5 ± 1.8	1.06 ± 0.12	-	-
Nova Sco 94	226.1 ± 0.8	3.14 ± 0.03	86 ± 4	-141.9 ± 1.3	3.20 ± 0.50	-3.3 ± 0.5	-4.0 ± 0.4
XTE J1118	708.8 ± 1.4	6.27 ± 0.04	100 ⁺³ ₋₁₁	2.7 ± 1.1	1.70 ± 0.10	-16.8 ± 1.6	-7.4 ± 1.6

*References: V404 Cygni: Casares (1996), Casares (2007), Miller-Jones et al. (2009b), Khargharia et al. (2010); Centaurus X-4: González Hernández et al. (2005), Casares et al. (2007), Khargharia et al. (2010); A0620-00: Neilsen et al. (2008), González Hernández & Casares (2010), Cantrell et al. (2010); Nova Scorpii 1994: Hjellming & Rupen (1995), Orosz & Bailyn (1997), Mirabel et al. (2002), González Hernández et al. (2008a), and this work; XTE J1118+480: Mirabel et al. (2001), Gelino et al. (2006), González Hernández et al. (2008b).

NOTE.—Kinematical and dynamical properties, orbital parameters and proper motions of low-mass X-ray binaries.

TABLE 5
STELLAR, VEILING PARAMETERS AND CHEMICAL ABUNDANCES IN LMXBS

Name*	A0620-00	Centaurus X-4	XTE J1118+480	Nova Sco 94	V404 Cygni [†]
Alternative name	V616 Mon	V822 Cen	-	GRO J1655-40	GS 2023+338
T_{eff} (K)	4900 ± 100	4500 ± 100	4700 ± 100	6100 ± 200	4800 ± 100
$\log(g/\text{cm s}^2)$	4.2 ± 0.3	3.9 ± 0.3	4.6 ± 0.3	3.7 ± 0.2	3.50 ± 0.15
f_{4500}	0.25 ± 0.05	1.85 ± 0.10	0.85 ± 0.20	0.15 ± 0.05	0.15 ± 0.05
$m_0/10^{-4}$	-1.4 ± 0.2	-7.1 ± 0.3	-2 ± 1	-1.2 ± 0.3	-1.3 ± 0.2
[O/H] [‡]	-	-	-	0.91 ± 0.09	0.60 ± 0.19
[Na/H]	-	-	-	0.31 ± 0.26	0.30 ± 0.19
[Mg/H]	0.40 ± 0.16	0.35 ± 0.17	0.35 ± 0.25	0.48 ± 0.15	0.00 ± 0.11
[Al/H]	0.40 ± 0.12	0.30 ± 0.17	0.60 ± 0.20	0.05 ± 0.18	0.38 ± 0.09
[Si/H]	-	-	0.37 ± 0.21	0.58 ± 0.08	0.36 ± 0.11
[S/H]	-	-	-	0.66 ± 0.12	-
[Ca/H]	0.10 ± 0.20	0.21 ± 0.17	0.15 ± 0.23	-0.02 ± 0.14	0.20 ± 0.16
[Ti/H]	0.37 ± 0.23	0.40 ± 0.17	0.32 ± 0.26	0.27 ± 0.22	0.42 ± 0.20
[Cr/H]	-	-	-	-	0.31 ± 0.19
[Fe/H]	0.14 ± 0.20	0.23 ± 0.10	0.18 ± 0.17	-0.11 ± 0.10	0.23 ± 0.09
[Ni/H]	0.27 ± 0.10	0.35 ± 0.10	0.30 ± 0.21	0.00 ± 0.21	0.21 ± 0.19

*References: V404 Cygni: This work; Centaurus X-4: González Hernández et al. (2005), González Hernández et al. (2007); A0620-00: González Hernández et al. (2004), González Hernández et al. (2007); Nova Scorpii 1994: González Hernández et al. (2008a); XTE J1118+480: González Hernández et al. (2008b)

[†]The uncertainties on the stellar abundances given in this table has been derived without taking into the error on the microturbulence (see Table 2).

[‡]Oxygen abundances are given in NLTE.

NOTE.—Stellar and veiling parameters, and chemical abundances of secondary stars in low-mass X-ray binaries.

spectroscopic determinations in Table 5. Using Kepler’s third law, we have estimated the current orbital separation, $a_{c,f}$, from the orbital period, P_{orb} , and the reported masses of the compact object, $M_{\text{CO},f}$, and the companion star, $M_{2,f}$. The ratio of the radius of the Roche lobe, R_L , and the orbital separation can be estimated using Eggleton’s expression (Eggleton 1983) as

$$R_L/a_{c,f} = 0.49q^{2/3}/[0.6q^{2/3} + \ln(1 + q^{1/3})].$$

Assuming that the star is filling its Roche lobe, $R_L = R_{2,f}$, and using the mass of the secondary star, we derive the expected surface gravity.

From Table 5 one can see that in general, the spectroscopic determinations are close to values derived from the size of the Roche lobe of the secondary star. In particular, for Centaurus X-4, A0620-00, and XTE J1118+480, the values are consistent within the 1σ uncertainties, and for Nova Sco 94 at 1.2σ . However, for V404 Cygni, the surface gravity is only compatible at the 5σ level, given the relatively small uncertainty in the spectroscopic surface gravity. On the other hand, we note that surface gravities derived from the size of the Roche lobe strongly depend on the current masses of the compact object and the secondary star, and thus depend on the estimated, sometimes uncertain, orbital inclination. We note, for instance, the case of A0620-00, whose black hole mass estimate has changed over the last ten years from $11.0 \pm 1.9 M_\odot$ (Gelino et al. 2001), to $9.7 \pm 0.6 M_\odot$ (Froning et al. 2007), and finally to $6.61 \pm 0.25 M_\odot$ (Cantrell et al. 2010). However, for the case of V404 Cygni, the mass ratio and the orbital period have been determined with high precision (see Table 5), leaving little room to increase the value of the surface gravity obtained from the secondary’s mass and the size of the Roche lobe. Thus, adopting larger masses (Shahbaz et al. 1994) for the compact object, $M_{\text{CO},f} = 12 M_\odot$, and the companion star, $M_{2,f} = 0.7 M_\odot$, the result does not change significantly; the estimated surface gravity would be $\log g_{R_L} = 2.72 \pm 0.13$. Therefore, a possible uncertain orbital inclination does not seem to be the reason for this disagreement.

3.2. Stellar Abundances

We inspected several regions in the observed Keck/HIRES spectrum of the secondary star,

searching for suitable lines for a detailed chemical analysis. Using the derived stellar parameters, we first determined the Fe abundance by comparing synthetic spectra with each individual feature in the HIRES spectrum (see Table 2). In Figure 3 we display one of the spectral regions analyzed to obtain the Fe abundance, also showing the best synthetic spectral fit to the observed spectrum of a template star (HIP 64797 with $T_{\text{eff}} = 4970$ K, $\log g = 4.33$, and $[\text{Fe}/\text{H}] = -0.24$ dex). We only use as abundance indicators those features which are well reproduced in the template star. The chemical analysis is summarized in Table 2. The errors in the element abundances show their sensitivity to the uncertainties in the effective temperature (ΔT_{eff}), gravity ($\Delta_{\log g}$), veiling (Δ_{vel}), microturbulence (Δ_ξ), and the dispersion of the measurements from different spectral features (Δ_σ). In Table 2 we also state the number of features analyzed for each element. The uncertainties Δ_σ were estimated as $\Delta_\sigma = \sigma/\sqrt{N}$, where σ is the standard deviation of the N measurements. The uncertainties ΔT_{eff} , Δ_ξ , $\Delta_{\log g}$, and Δ_{vel} were determined in the same way as, for instance, in the T_{eff} case: $\Delta T_{\text{eff}} = (\sum_{i=1}^N \Delta T_{\text{eff},i})/N$. The total uncertainty given in Table 2 was derived using the following expression:

$$\Delta[\text{X}/\text{H}] = \sqrt{\Delta_\sigma^2 + \Delta_{T_{\text{eff}}}^2 + \Delta_{\log g}^2 + \Delta_\xi^2 + \Delta_{\text{vel}}^2}.$$

In Figure 4 we show the spectral region 5910–5955 Å, where there are some Ti and Si lines used to derive their abundances. In this region there are also some telluric lines, with equivalent widths of ~ 30 mÅ, which are significantly weaker than the stellar features, whose equivalent widths are ~ 250 mÅ, and we do not think these lines have caused any problem in the abundance determination. This spectral region contains two Fe features at ~ 5914.2 and ~ 5916.3 Å which are sensitive to surface gravity variations. One can easily notice the relative different strengths of both Fe features in the template spectra (with $\log g \approx 4.3$) and in the secondary star in V404 Cygni (with $\log g \approx 3.5$).

3.3. Oxygen

The oxygen abundance was derived from the O I triplet at 7771–5 Å, which for the relatively high rotation velocity of the secondary star in V404 Cygni produces two well-resolved features

that we have analyzed independently. In Figure 5 we show the 7755–7820 Å range, where the O I features in the secondary star appear to be apparently enhanced when compared with those in the template star having similar effective temperature. The best fit in LTE gives an oxygen abundance of $[O/H]_{\text{LTE}} \approx 0.8$. We note that the atomic data for O I lines were adopted from Ecuivillon et al. (2006). These authors slightly modified the oscillator strengths in order to obtain a solar oxygen abundance of $\log \epsilon(O)_{\odot} = 8.74$. For other elements we assumed as solar abundances those given by Grevesse et al. (1996).

The O I $\lambda 7771$ –5 triplet suffers from appreciable non-LTE (NLTE) effects (see, e.g., Ecuivillon et al. 2006). For the stellar parameters and oxygen abundance of the secondary star, NLTE corrections¹ are estimated to be ~ -0.20 dex for the NIR O I $\lambda 7771$ –5 triplet. Table 2 provides the oxygen abundance properly corrected for NLTE effects.

In principle, one could argue that the relatively “high” value for the spectroscopic surface gravity found in this work (see §3.1) for V404 Cygni may affect the derived abundances. We note that the spectroscopic values were derived for the secondary star at nearly inferior conjunction, which means that we are looking at the “spherical” side of the Roche-lobe-like star. Therefore, the derived T_{eff} and $\log g$ values should be larger than the mean T_{eff} and $\log g$ values of the star (see Table 5), although this would only account for 100 K and 0.1 dex, respectively.

In Table 2 one can see that the NIR O I lines are sensitive to the surface gravity, with a change of 0.06 dex in derived abundance for a change of +0.15 dex in $\log g$. This means that for a surface gravity as low as $\log g = 2.7$, one would obtain a 0.32 dex lower oxygen abundance. On the other hand, the Fe abundance would not be sensitive to this change in surface gravity, and therefore we would get $[O/Fe]_{\text{NLTE}} = 0.05$ dex.² We also note that, for instance, a 300 K lower T_{eff} would re-

sult in a substantial increase in the derived oxygen abundance, ~ 0.48 dex (see Table 2), and a smaller decrease in the Fe abundance, ~ -0.15 dex, yielding $[O/Fe]_{\text{NLTE}} = 1$ dex with $[Fe/H] = 0.08$. These values have been estimated without taking into account the possibly smaller NLTE correction at the lower value of T_{eff} .

3.4. Magnesium

The magnesium abundance was derived from eight Mg I features, including the four optical lines of the Mg I b $\lambda 5167$ –83 Å triplet and Mg I $\lambda 5528$ Å. These Mg I lines are known to be sensitive to NLTE effects (see, e.g., Zhao et al. 1998), although with NLTE corrections of only $\sim +0.05$ in the Sun and probably smaller ones at these cooler temperatures (Zhao & Gehren 2000).

We note here that we are applying an automatic 1.5σ abundance rejection over the initial set of lines, slightly affecting the Mg abundance. This discards two Mg I features, lowering the Mg abundance by 0.06 dex and decreasing the standard deviation of the measurements from 0.15 to 0.09 dex. For other elements like Si and Ti, the 1.5σ rejection yields 0.04 lower and 0.03 higher abundance, respectively, with a decrease of the standard deviation by only 0.02 dex.

Finally, possible differences in the stellar parameters also have an impact on the Mg abundance (see Table 2). The Mg I lines are sensitive to the effective temperature and surface gravity, with a change of 0.06 and -0.03 dex in derived abundance for changes of 100 K in T_{eff} and +0.15 dex in $\log g$, respectively. In this case, 300 K lower T_{eff} would result in 0.18 dex lower Mg abundance, whereas a decrease of 0.8 dex in $\log g$ would give rise to a 0.16 dex higher Mg abundance.

4. Discussion

The global metallicity of the secondary star in V404 Cygni is slightly higher than solar, similar to that of the secondary star in other black hole X-ray binaries such as A0620–00 and XTE J1118+480, but also comparable to that of many stars in the solar neighborhood. We have searched for anomalies in the abundance pattern of the secondary star in comparison with typical abundances of stars belonging to the Galactic thin disk. The abundances of other elements relative to iron listed in Table 2

¹ $\Delta_{\text{NLTE}} = \log \epsilon(X)_{\text{NLTE}} - \log \epsilon(X)_{\text{LTE}}$.

²Fe lines are indeed quite sensitive to variations of the surface gravity, typically with changes of ± 0.05 dex in Fe abundance for a change of +0.15 dex in $\log g$, although some Fe lines would not show any change in abundance. However, these differences compensate each other, so that the average change is ~ 0.001 dex, almost null.

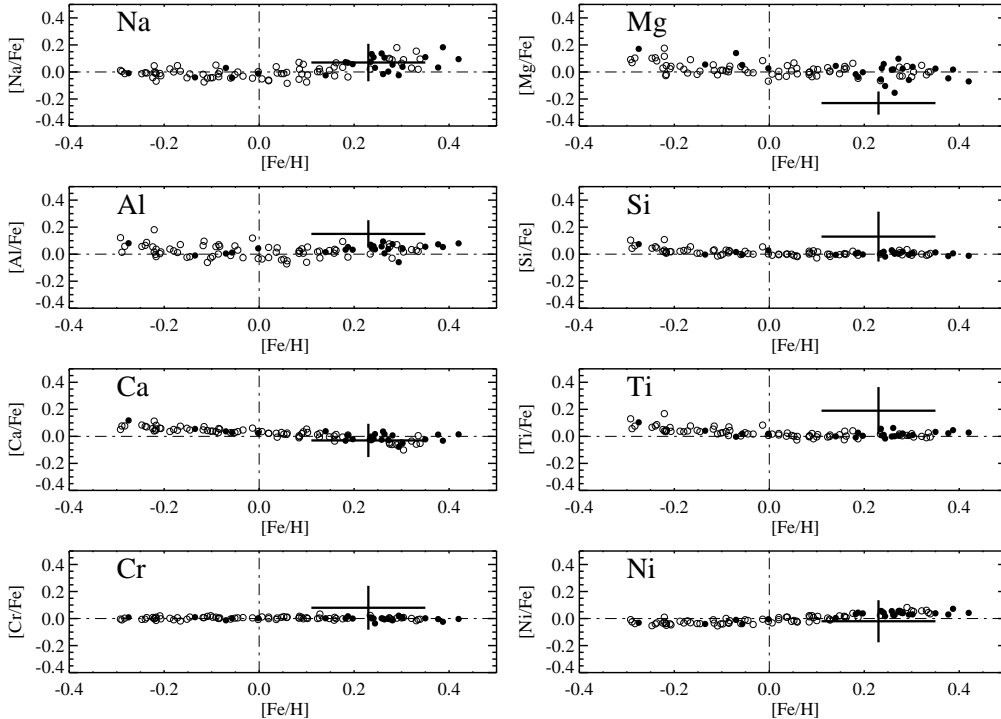


Fig. 6.— Abundance ratios of the secondary star in V404 Cygni (blue wide cross) in comparison with the abundances of solar-type metal-rich dwarf stars. Galactic trends were taken from González Hernández et al. (2010). The size of the cross indicates the uncertainty. Filled and empty circles correspond to abundances for exoplanet host stars and stars without known exoplanet companions, respectively. The dashed-dotted lines indicate solar abundance values.

are compared in Figures 6 and 7 with the Galactic trends of these elements in the relevant range of metallicities. We adopted recent, very accurate Galactic trends from González Hernández et al. (2010) for all elements except for oxygen, because we needed O abundances measured from the NIR O I triplet. We thus decided to adopt the Galactic trend of oxygen published by Ecuivillon et al. (2006). Figures 6 and 7 show moderate anomalies for Ti, Al, and Si in the secondary star in V404 Cygni, and whereas Mg is surprisingly underabundant, oxygen appears to be enhanced in comparison with the galactic trend.

Table 6 shows the element abundance ratios in V404 Cygni and the average values in stars with iron content in the range $0.11 < [\text{Fe}/\text{H}] < 0.35$, the comparison sample corresponding to a 1σ uncertainty in the iron abundance of the secondary star. The elements Na, Si, Ca, Cr, and Ni are consistent with the average values in thin-disk stars within the error bars. Mg appears to be underabundant, whereas Al and Ti are roughly consistent at 1σ .

Oxygen may be considered separately since it is clearly more abundant, at 2.8σ , than the average values of the thin-disk stars.

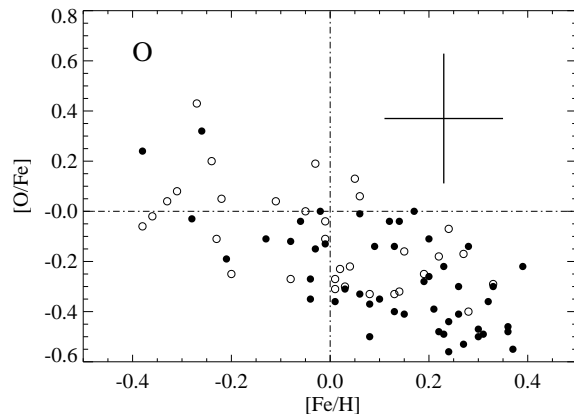


Fig. 7.— The same as in Fig. 6 but for oxygen. Galactic trends were taken from Ecuivillon et al. (2006).

V404 Cygni is located in a Galactic thin-disk

TABLE 6
ELEMENT ABUNDANCE RATIOS IN V404 CYGNI

Element	$[X/Fe]_{V404Cyg}$	$\Delta_{[X/Fe],V404Cyg}^*$	$[X/Fe]_{stars}$	σ_{stars}	$\Delta_{\sigma,stars}$
O	0.37	0.24	-0.32	0.19	0.033
Na	0.07	0.14	0.05	0.05	0.009
Mg	-0.23	0.09	0.00	0.05	0.008
Al	0.15	0.11	0.04	0.03	0.006
Si	0.13	0.15	0.00	0.01	0.002
Ca	-0.03	0.12	-0.02	0.03	0.005
Ti	0.19	0.17	0.01	0.02	0.003
Cr	0.08	0.16	0.00	0.01	0.001
Ni	-0.02	0.15	0.03	0.02	0.003

*Uncertainties in the element abundance ratios ($[X/Fe]$) in the secondary star in V404 Cygni.

NOTE.— $[X/Fe]_{stars}$ indicates the average value of 36 stars with iron content in the range 0.11 to 0.35 corresponding to the abundance range $[Fe/H] \pm \sigma_{Fe}$ of the secondary star in V404 Cygni, taken from Ecuivillon et al. (2006) and González Hernández et al. (2010). The uncertainty in the average value of an abundance ratio in the comparison sample is obtained as $\Delta_{\sigma,stars} = \sigma_{stars}/\sqrt{N}$, where σ_{stars} is the standard deviation of the measurements and N is the number of stars.

region at a distance $d = 2.39 \pm 0.14$ kpc from the Sun (Miller-Jones et al. 2009b), but its peculiar velocity is larger than the intrinsic velocity dispersion in the Galactic plane. Miller-Jones et al. (2009b) argue that this peculiar velocity, $v_{pec} = 39.9 \pm 5.5$ km s $^{-1}$, may be the result of the natal kick from the mass ejection in the SN/HN explosion of the primary star in this LMXB. The companion star could have captured a significant amount of the ejected matter in the SN/HN explosion that formed the compact object. We have explored this possibility with the aim of obtaining information on the chemical composition of the progenitor of the compact object.

4.1. Spherical Explosion

The secondary star in V404 Cygni may have lost a significant amount of its initial mass through a mass-transfer mechanism onto the compact object, during the binary evolution. Its post-SN evolution has been studied in detail by Miller-Jones et al. (2009a). These authors suggest that from 0.5 to 1.5 M_{\odot} may have been accreted from the companion star. We estimated the current mass of the secondary star at $M_{2,f} = 0.54 \pm 0.08 M_{\odot}$ (see Table 5), from the current black hole mass $M_{BH,f} = 9.0 \pm 0.6 M_{\odot}$ (Khargharia et al. 2010) and mass ratio $q_f = 0.060 \pm 0.005$ (Casares & Charles

1994). Following Miller-Jones et al. (2009a), we assume an initial mass for the secondary star of $M_{2,i} \approx 2 M_{\odot}$ and an initial black hole mass of $M_{BH,i} \approx 8 M_{\odot}$. Therefore, the final mass of the black hole would be $M_{BH,f} \approx 9.5 M_{\odot}$ which is consistent with the current estimate of the black hole mass (Khargharia et al. 2010).

The high O content in this companion star may not suggest any strong CNO processing within the star itself during its evolution, since this would increase the N abundance (see, e.g., Haswell et al. 2002). Oxygen, however, is not expected to decrease too much compared with C (Clayton 1983). Therefore, the CNO-processed material is C underabundant and N overabundant. Unfortunately, in the Keck/HIRES optical spectrum of the secondary star there are no sufficiently strong and unblended stellar lines to provide an accurate and reliable C abundance. Khargharia et al. (2010) argued that their NIR spectrum of V404 Cygni suggests that CO molecules seems to fit well with a solar-abundance K3 III template spectrum for which they adopt $T_{eff} \approx 4300$ K. We note here that CO molecular bands are more sensitive to the C abundance than to the O abundance and are stronger at lower effective temperatures. Thus, their argument do not necessarily contradict our determination of the O abundance.

The present orbital distance is $a_{c,f} \approx 31 R_{\odot}$ (see

Table 5). We will assume that the post-SN orbital separation after tidal circularization of the orbit was $a_{c,i} \approx 15 R_{\odot}$, since the secondary must have experienced mass and angular momentum losses during the binary evolution until it reached its present configuration. Similarly to the case of XTE J1118+480 (González Hernández et al. 2008b), we can estimate the maximum ejected mass in the SN/HN explosion. A binary system such as V404 Cygni will survive a spherical SN explosion if the ejected mass $\Delta M = M_{\text{He}} - M_{\text{BH},i} \leq (M_{\text{He}} + M_{2,i})/2$ (Hills 1983). This implies a mass of the He core before the SN explosion of $M_{\text{He}} \leq 18 M_{\odot}$. We therefore adopt He core masses of $M_{\text{He}} \approx 15\text{--}16 M_{\odot}$, so we infer a He core radius of $R_{\text{He}} \approx 3 R_{\odot}$ from the expression in Portegies Zwart et al. (1997a, and references therein).

Assuming a pre-SN circular orbit and an instantaneous spherically symmetric ejection (that is, shorter than the orbital period), one can estimate the pre-SN orbital separation, a_0 , using the relation given by van den Heuvel & Habets (1984): $a_0 = a_{c,i} \mu_f$, where $\mu_f = (M_{\text{BH},i} + M_{2,i})/(M_{\text{He}} + M_{2,i})$. We find $a_0 \approx 9$, for the adopted values of $M_{\text{He}} = 15 M_{\odot}$ and $a_{c,i} = 15 R_{\odot}$. At the time of the SN explosion ($\sim 5\text{--}6$ Myr; Brunish & Truran 1982), a $2 M_{\odot}$ secondary star, still in its pre-main-sequence evolution, has a radius $R_{2,i} \approx 3.3 R_{\odot}$. The material possibly captured by the secondary star in the SN/HN event has a much larger mean molecular weight than the pre-explosion gas of the secondary star, so it has probably been well mixed within the star by thermohaline mixing in a relatively short timescale (Podsiadlowski et al. 2002, and references therein). Therefore, the subsequent loss of material from the secondary star onto the compact object should not affect the chemical composition of its atmosphere. The amount of mass deposited on the secondary can be estimated as $m_{\text{cap}} = \Delta M (\pi R_{2,i}^2 / 4\pi a_0^2) f_{\text{cap}} M_{\odot}$, where f_{cap} is the fraction of mass, ejected within the solid angle subtended by the secondary star, that is eventually captured. We assume that the captured mass, m_{cap} , is completely mixed with the rest of the companion star.

We compute the expected abundances in the atmosphere of the secondary star after the pollution from the progenitor of the compact object as in González Hernández et al. (2004)

and González Hernández et al. (2008b). We use $40 M_{\odot}$ spherically symmetric core-collapse explosion models ($M_{\text{He}} \approx 15.1 M_{\odot}$) at solar metallicity ($Z = 0.02$) and for two different explosion energies (Umeda & Nomoto 2002, 2005; Tominaga et al. 2007). These models imply $\Delta M \approx 7 M_{\odot}$ and need small capture efficiencies of $f_{\text{cap}} \lesssim 0.1$ (i.e., 10%) to increase significantly the metal content of the secondary star. In order to fix the f_{cap} parameter, we have tried to get an expected Al abundance, $[\text{Al}/\text{H}] \approx 0.45$, consistent with the observed Al abundance within the error bars. These model computations are shown in Table 7. These models would also provide a different mass fraction of each element at each value of the mass cut (defined as the mass that initially collapsed to form the compact remnant). For more details of the models, see Tominaga et al. (2007).

The assumptions regarding the initial mass and the post-SN orbital distance of the secondary star are not so relevant due to the free parameter f_{cap} . A different value for the initial mass of the secondary star, as small as (say) $1 M_{\odot}$ with an initial radius of $R_{2,i} \approx 1.3 R_{\odot}$ at the time of the SN explosion, and for the post-SN orbital separation, say $a_{c,i} = 25 R_{\odot}$, would require a larger capture efficiency factor of $f_{\text{cap}} \approx 0.45$ (i.e., 45%).

The explosion energy is $E_K = 1 \times 10^{51}$ erg and $E_K = 30 \times 10^{51}$ erg for the SN and HN models, respectively. This energy is deposited instantaneously in the central region of the progenitor core to generate a strong shock wave. The subsequent propagation of the shock wave is followed through a hydrodynamic code (Umeda & Nomoto 2002, and references therein). As in González Hernández et al. (2008b), our model computations assume different mass cuts and fallback masses, and a mixing factor of 1 which assumes that all fallback matter is well mixed with the ejecta. The amount of fallback, M_{fall} , is the difference between the final remnant mass, $M_{\text{BH},i}$, and the initial remnant mass of the explosion, M_{cut} . We should recall here the ejected mass, ΔM , which is equal to $M_{\text{He}} - M_{\text{BH},i}$, where M_{He} is the mass of the He core.

We use SN/HN models to provide us with the yields of the explosion before radiative decay of element species. We then compute the integrated, decayed yields of the ejecta by adopting a mass cut and by mixing all of the material above the

mass cut. Finally, we calculate the composition of the matter captured by the secondary star, and we mix it with the material of its convective envelope. It has been suggested that the black hole in the LMXB Nova Sco 1994 could have formed in a two-stage process where the initial collapse led to the formation of a neutron star accompanied by a substantial kick and the final mass of the compact remnant was achieved by matter that fell back after the initial collapse (Podsiadlowski et al. 2002). However, the black hole mass in that system has been estimated at $\sim 5.4 M_{\odot}$ (Beer & Podsiadlowski 2002) or $\sim 6.6 M_{\odot}$ (Shahbaz 2003, see Table 5), while the black hole in V404 Cygni may have an initial mass of $\sim 8 M_{\odot}$ which would require a fallback mass of $\sim 6.6 M_{\odot}$ if we assume $\sim 1.4 M_{\odot}$ for a canonical neutron star. MacFadyen et al. (2001) proposed a scenario where collapsar models harbor black holes that could form in a mild explosion with substantial fallback (up to $\sim 5 M_{\odot}$).

In Figure 8 we show the expected abundances of the secondary star after contamination from the nucleosynthetic products of the SN explosion ($E_K = 1 \times 10^{51}$ erg) of a $M_{\text{He}} \approx 15 M_{\odot}$ progenitor star. The initial abundances of the secondary star have been estimated from the average abundances of thin-disk solar-type stars with $[\text{Fe}/\text{H}] \approx 0.23$ (González Hernández et al. 2010), which are provided in Table 7. Note that for a given model, the Al abundance in the secondary star hardly depends on the mass cut, since Al forms in the outer layers of the explosion. Thus, once the capture efficiency is fixed, the Al abundance in Figure 8 is almost constant.

The expected abundances of O, Mg, and Al in the secondary star after contamination from the SN ejecta remain mostly independent of the adopted mass cut, whereas other elements like Si, Ca, Ti, Fe, and Ni are quite sensitive to the mass cut of the model. This appears to be more clear in the HN model, where the higher explosion energy enhances the amounts of the α -process elements Si, Ca, and Ti. The Fe-group elements like Cr, Fe, and Ni are also sensitive to the mass cut, especially in the HN model.

For both the SN model (left panel in Fig. 8) and the HN model (right panel in Fig. 8), the predicted abundances agree with the observed abundances in the secondary star relatively well, except

for those of O and Mg. The expected Mg abundance is too high in comparison with the observed value since the adopted initial Mg abundance is already higher than the observed abundance (see Table 7). The case of O is just the contrary; the initial abundance is so low that it is not possible to reach the observed O abundance when fitting other element abundances (see Fig. 8).

For mass cuts above $\sim 3 M_{\odot}$, very little Si, Ca, Ti, Fe, Cr, and Ni is ejected; thus, the expected abundances of the model essentially reflect the initial abundances of the secondary star. In contrast, O, Na, Mg, and Al are hardly sensitive to the mass cut, and all are enhanced due to the capture of enriched material in the SN/HN explosion.

We could have also investigated a model with solar initial abundances for the secondary star ($[\text{X}/\text{H}]_0 = 0$) and the same explosion model of solar metallicity ($Z = 0.02$), although it is unlikely that a significant amount of elements formed in the inner layers of the explosion (such as Ti, Ni, and Fe) would be present in the ejecta. In such models, only the HN explosion with a mass cut as low as $M_{\text{cut}} \approx 2 M_{\odot}$ would fit the relatively enhanced observed abundances of Si, Ti, Cr, Fe, and Ni, but we would still not be able to fit the O and Mg abundances. This low mass cut would require very efficient mixing processes, and the model would also need a small capture efficiency of $f_{\text{cap}} \approx 0.15$ (i.e., only 15% of the matter ejected within the solid angle subtended by the secondary star).

4.2. Aspherical Explosion

Miller-Jones et al. (2009b) pointed out that due to the relatively small peculiar velocity of the system, V404 Cygni does not require an asymmetric kick. However, here we explore this possibility using explosion models from Maeda et al. (2002) that are not spherically symmetric. An aspherical SN explosion produces chemical inhomogeneities in the ejecta which are dependent on direction. Thus, if the jet in the aspherical SN explosion is collimated perpendicular to the orbital plane of the binary (for more details, see González Hernández et al. 2005), where the secondary star is located, elements such as Ti, Fe, and Ni are ejected mainly in the jet direction, while O, Mg, Al, Si, and S are preferentially ejected near the equatorial plane of the helium star

TABLE 7
METAL-RICH SUPERNOVA/HYPERNOVA EXPLOSION MODELS IN V404 CYGNI

Element	[X/H] Observed ^a	[X/H] ₀ ^b	[X/H] Expected ^d			
			$M_{\text{cut,low}}^{\text{c}}$	$M_{\text{cut,up}}$	$M_{\text{cut,low}}$	$M_{\text{cut,up}}$
Spherical explosion model of $Z = 0.02$						
			Supernova		Hypernova	
O	0.60	-0.09	0.13	0.12	0.13	0.12
Na	0.30	0.29	0.56	0.56	0.50	0.56
Mg	0.00	0.24	0.35	0.34	0.35	0.34
Al	0.38	0.27	0.46	0.45	0.44	0.45
Si	0.36	0.24	0.30	0.25	0.34	0.25
Ca	0.20	0.22	0.26	0.22	0.29	0.22
Ti	0.42	0.25	0.28	0.25	0.35	0.25
Cr	0.31	0.24	0.28	0.24	0.31	0.24
Fe	0.23	0.23	0.32	0.23	0.34	0.23
Ni	0.21	0.27	0.41	0.28	0.39	0.28
Aspherical explosion model with $Z = 0.02$						
			Angle ^e = 0°–15°		Angle = 0°–90°	
O	0.60	-0.09	0.17	0.14	0.19	0.19
Na	0.30	0.29	0.39	0.38	0.38	0.39
Mg	0.00	0.24	0.36	0.35	0.36	0.37
Al	0.38	0.27	0.45	0.43	0.45	0.46
Si	0.36	0.24	0.31	0.28	0.39	0.33
Ca	0.20	0.22	0.24	0.22	0.33	0.27
Ti	0.42	0.25	0.25	0.25	0.41	0.35
Cr	0.31	0.24	0.24	0.24	0.33	0.29
Fe	0.23	0.23	0.23	0.23	0.31	0.26
Ni	0.21	0.27	0.27	0.27	0.40	0.33

^aObserved abundances of the secondary star in V404 Cygni.

^bInitial abundances assumed for the secondary star in V404 Cygni; see text.

^c $M_{\text{cut,low}}$ and $M_{\text{cut,up}}$ are (respectively) the lower and upper mass cuts adopted in the model computation. See the exact value in the captions of Figs. 12 and 13.

^dExpected abundances of the secondary star.

^eAngular range, measured from the equatorial plane, in which all the ejected material in the explosion has been completely mixed for each velocity point.

NOTE.—Expected abundances in the secondary atmosphere contaminated with nucleosynthetic products of metal-rich explosion models for two different mass cuts and symmetries, presented in Figs. 12 and 13.

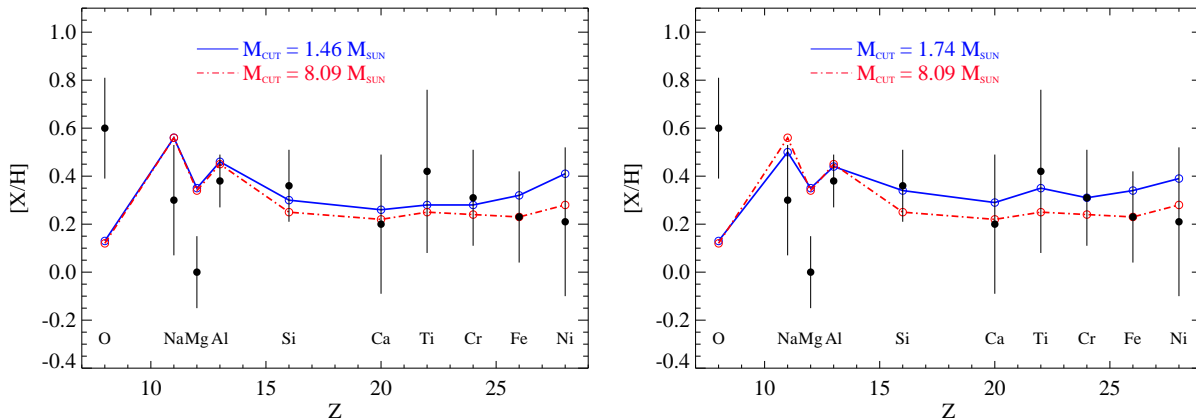


Fig. 8.— *Left panel*: Observed abundances (filled circles with error bars) in comparison with the expected abundances in the secondary star of V404 Cygni after having captured 10% of the matter ejected within the solid angle subtended by the secondary from a solar metallicity ($Z = 0.02$) $40 M_{\odot}$ spherically symmetric supernova explosion ($M_{\text{He}} = 15.1 M_{\odot}$) with $E_K = 1 \times 10^{51}$ erg for two different mass cuts, $M_{\text{cut}} = 1.46 M_{\odot}$ (solid line with open circles) and $M_{\text{cut}} = 8.09 M_{\odot}$ (dashed-dotted line with open circles). The initial abundances of the secondary star were adopted for the average abundances of thin-disk solar-type stars with $[\text{Fe}/\text{H}] = 0.23 \pm 0.12$. *Right panel*: Same as left panel, but for a spherically symmetric hypernova explosion ($E_K = 30 \times 10^{51}$ erg) for two different mass cuts, $M_{\text{cut}} = 1.74 M_{\odot}$ (solid line with open circles) and $M_{\text{cut}} = 8.09 M_{\odot}$ (dashed-dotted line with open circles).

(Maeda et al. 2002).

In Figure 9 we compare the predicted abundances in the atmosphere of the secondary star after pollution from an aspherical explosion model of a metal-rich progenitor having a $16 M_{\odot}$ He core (see also Table 7). The initial abundances of the secondary were, as in the spherical case, equally extracted from the average values of solar-type stars of the solar neighborhood with similar iron content (see Table 7). The left panel of Figure 9 reflects the composition of the material ejected in the equatorial plane, which should be rich in O, Na, Mg, Al, and Si — the only elements significantly enhanced with respect to the initial abundances. We see that the choice of the mass cut does not make a significant difference, and as in the spherical case, this model fits all of the element abundances within their error bars except for O and Mg.

In the right panel of Figure 9 we have considered complete lateral mixing (Podsiadlowski et al. 2002) — that is, the ejected matter is completely mixed within each velocity bin (for more details, see González Hernández et al. 2008b). The observed abundances might be better reproduced if complete lateral mixing is adopted, since this process tends to enhance the Si, Ca, Ti, Cr, Fe, and

Ni element abundances at all mass cuts. A model with solar initial abundances for the secondary star (i.e., $[\text{X}/\text{H}]_0 = 0$) and the same explosion model of solar metallicity ($Z = 0.02$) was also inspected, providing the same result except for the equatorial model, which produces too low abundances of Ti, Fe, and Ni in comparison with the observations.

5. Conclusions

We have presented Keck I/HIRES high-resolution spectroscopy of the black hole X-ray binary V404 Cygni. The spectra were obtained at system orbital phase close to zero to minimize the effect of the Roche-lobe symmetry of the secondary star. We have performed a detailed chemical analysis of the secondary star, applying a technique that provides a determination of the stellar parameters and takes into account any possible veiling from the accretion disk. We find $T_{\text{eff}} = 4800 \pm 100$ K, $\log[g/\text{cm s}^2] = 3.50 \pm 0.15$, $[\text{Fe}/\text{H}] = 0.23 \pm 0.19$, and a disk veiling (defined as $F_{\text{disk}}/F_{\text{total}}$) of $\sim 5\%$ at 5100 \AA , decreasing toward longer wavelengths.

We have derived the chemical abundances of O, Na, Mg, Al, Si, Ca, Ti, Cr, Fe, and Ni. They are typically higher than solar, and some elements show additional slight enhancements (e.g., Al, Si,

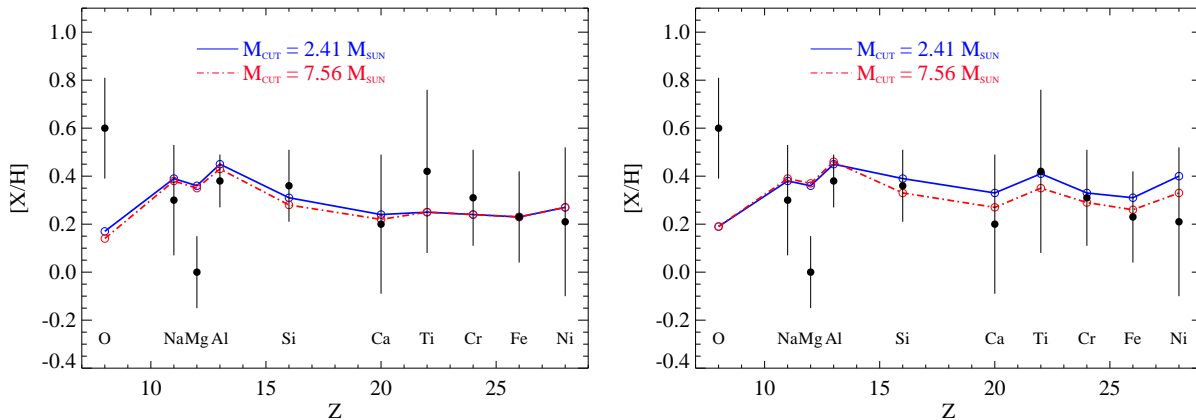


Fig. 9.— *Left panel*: Observed abundances (filled circles with error bars) in comparison with the expected abundances in the secondary star of V404 Cygni after having captured $\sim 10\%$ of the matter ejected within the solid angle subtended by the secondary from an aspherical SN explosion of $E_K = 10 \times 10^{51}$ erg for two different mass cuts, $M_{\text{cut}} = 2.41 M_{\odot}$ (solid line with open circles) and $M_{\text{cut}} = 7.56 M_{\odot}$ (dashed-dotted line with open circles). This model corresponds to the matter ejected in the equatorial plane of the primary, where we assumed that the secondary star is located (for more details, see González Hernández et al. 2005). *Right panel*: Same as left panel, but in this model we have assumed complete lateral mixing, where all of the material within given velocity bins is completely mixed. Two simulations are shown for two different mass cuts, $M_{\text{cut}} = 2.41 M_{\odot}$ (solid line with open circles) and $M_{\text{cut}} = 7.56 M_{\odot}$ (dashed-dotted line with open circles).

and Ti). The O abundance was derived using the O I triplet at $7771\text{-}5 \text{ \AA}$, a robust O abundance indicator; it appears to be a factor of 4 more abundant than in the Sun, and more than a factor of 2 overabundant in comparison with stars of the solar neighborhood having similar iron content. These photospheric abundances suggest possible contamination from nucleosynthetic products in the supernova/hypernova explosion that formed the compact object in this system.

The peculiar velocity of the LMXB V404 Cygni, $v_{\text{pec}} = 39.9 \pm 5.5 \text{ km s}^{-1}$, is larger than the Galactic velocity dispersion, suggesting that the black hole in this system formed in a supernova event. Thus, the secondary star could have kept a record of this SN/HN event in the chemical composition of its atmosphere. We explored this possibility using a variety of SN/HN explosion models for different geometries. We compared the expected abundances in the companion star after contamination of nucleosynthetic products from initial metallicities of the secondary star adopted using the average values in solar-type thin-disk stars. Metal-rich spherically symmetric models are able to reproduce the observed abundances relatively well, except for O and Mg, which appear to show too high and too low (respectively) abundances in comparison to model predictions, regardless of the

choice of the mass cut.

A spherical explosion easily provides the energy required to explain the peculiar velocity of this system, which is in the Galactic plane. Therefore, an asymmetric SN/HN explosion may not be required. However, we have also modelled the expected abundances in the secondary star after capturing a significant amount of material from an aspherical explosion. These models also provide good agreement for all elements, as in the spherical case, except for O and Mg, without invoking extensive fallback and mixing.

In a forthcoming paper (González Hernández et al. 2011, in preparation), we will present the Li abundance and study the ${}^6\text{Li}/{}^7\text{Li}$ isotopic ratio to explore different evolutionary scenarios and possible production of Li due to the X-ray radiation in this black-hole binary system (see Casares et al. 2007).

We thank K. Maeda, H. Umeda, K. Nomoto, and N. Tominaga for providing us with their spherical and aspherical explosion models. We are grateful to T. Marsh for the use of the MOLLY analysis package. J.I.G.H. acknowledges financial support from the Spanish Ministry of Science and Innovation (MICINN) under the 2009 Juan de la Cierva Programme. J.I.G.H. and G.I.

are grateful for financial support from MICINN grant AYA2008-04874, while J.C. acknowledges MICINN grant AYA2010-18080. Additional funding was provided by MICINN grant AYA2005-05149, and (to A.V.F.) by US National Science Foundation grant AST-0908886. The W. M. Keck Observatory is operated as a scientific partnership among the California Institute of Technology, the University of California, and NASA; it was made possible by the generous financial support of the W. M. Keck Foundation. This work has made use of the VALD database and IRAF facilities.

REFERENCES

- Allende Prieto, C., Barklem, P. S., Lambert, D. L., & Cunha, K. 2004, *A&A*, 420, 183
- Al-Naimiy, H. M. 1978, *Ap&SS*, 420, 183
- Blaauw, A. 1961, *Bull. Astron. Inst. Netherlands*, 15, 265
- Beer, M. E., & Podsiadlowski, P. 2002, *MNRAS*, 331, 351
- Benz, W., & Hills, J. G. 1992, *ApJ*, 433, 185
- Brunish, W. M., & Truran, J. W. 1982, *ApJS*, 49, 447
- Cantrell, A. G., et al. 2010, *ApJ*, 710, 1127
- Casares, J., Charles, P. A., & Naylor, T. 1992, *Nature*, 355, 614
- Casares, J., Charles, P. A., Naylor, T., & Pavlenko, E. P. 1993, *MNRAS*, 265, 834
- Casares, J., & Charles, P. A. 1994, *MNRAS*, 271, L5
- Casares, J. 1996, *IAU Colloq. 158: Cataclysmic Variables and Related Objects*, 208, 395
- Casares, J. 2007, *IAU Symposium*, 238, 3
- Casares, J., Bonifacio, P., González Hernández, J. I., Molaro, P., & Zoccali, M. 2007, *A&A*, 470, 1033
- Chen, B. 1997, *ApJ*, 491, 181
- Clayton, D. D. 1983, *Principles of Stellar Evolution and Nucleosynthesis* (Chicago: Univ. Chicago Press)
- Ecuivillon, A., Israelian, G., Santos, N. C., Shchukina, N. G., Mayor, M., & Rebolo, R. 2006, *A&A*, 445, 633
- Eggleton, P. P. 1983, *ApJ*, 268, 368
- Froning, C. S., Robinson, E. L., & Bitner, M. A. 2007, *ApJ*, 663, 1215
- Gelino, D. M., Harrison, T. E., & Orosz, J. A. 2001, *ApJ*, 122, 2668
- Gelino, D. M., Balman, Ş., Kiliiloğlu, Ü., Yilmaz, A., Kalemci, E., & Tomsick, J. A. 2006, *ApJ*, 642, 438
- González Hernández, J. I., Rebolo, R., Israelian, G., Casares, J., Maeder, A., & Meynet, G. 2004, *ApJ*, 609, 988
- González Hernández, J. I., Rebolo, R., Peñarrubia, J., Casares, J., & Israelian, G. 2005, *A&A*, 435, 1185
- González Hernández, J. I., Rebolo, R., Israelian, G., Casares, J., Maeda, K., Bonifacio, P., & Molaro, P. 2005, *ApJ*, 630, 495
- González Hernández, J. I., Rebolo, R., Israelian, G., Harlaftis, E. T., Filippenko, A. V., & Chornock, R. 2006, *ApJ*, 644, L49
- González Hernández, J. I., Rebolo, R., & Israelian, G. 2007, *IAU Symposium*, 238, 43
- González Hernández, J. I., Rebolo, R., & Israelian, G. 2008a, *A&A*, 478, 203
- González Hernández, J. I., Rebolo, R., Israelian, G., Filippenko, A. V., Chornock, R., Tominaga, N., Umeda, H., & Nomoto, K. 2008b, *ApJ*, 679, 732
- González Hernández, J. I., Iglesias-Groth, S., Rebolo, R., García-Hernández, D. A., Manchado, A., & Lambert, D. L. 2009, *ApJ*, 706, 866
- González Hernández, J. I., & Casares, J. 2010, *A&A*, 516, A58
- González Hernández, J. I., Israelian, G., Santos, N. C., Sousa, S., Delgado-Mena, E., Neves, V., & Udry, S. 2010, *ApJ*, 720, 1592
- González Hernández, J. I., Casares, J., Rebolo, R., Israelian, G., Filippenko, A. V., & Chornock, R. 2011, *ApJ*, in preparation

- Greene, J., Baily, C. D., & Orosz, J. A. 2001, *ApJ*, 554, 1290
- Grevesse, N., Noels, A., & Sauval, A. J. 1996, in *Cosmic Abundances*, ed. S. S. Holt & G. Sonneborn (San Francisco: ASP, Conf. Ser. Vol. 99), 117
- Haswell, C. A., Hynes, R. I., King, A. R., & Schenker, K. 2002, *MNRAS*, 332, 928
- Hills, J. G. 1983, *ApJ*, 267, 322
- Hills, J. G. 1991, *ApJ*, 102, 2
- Hjellming, R. M., & Rupen, M. P. 1995, *Nature*, 375, 464
- Hynes, R. I., Robinson, E. L., & Bitner, M. 2005, *ApJ*, 630, 405
- Hynes, R. I., Bradley, C. K., Rupen, M., Gallo, E., Fender, R. P., Casares, J., & Zurita, C. 2009, *MNRAS*, 399, 2239
- Israelian, G., Rebolo, R., Basri, G., Casares, J., & Martín, E. L. 1999, *Nature*, 401, 142
- Jonker, P. G., & Nelemans, G. 2004, *MNRAS*, 354, 355
- Khargharia, J., Froning, C. S., & Robinson, E. L. 2010, *ApJ*, 716, 1105
- Kifonidis, K., Plewa, T., Janka, H.-Th., & Müller, E. 2000, *A&A*, 531, L123
- Kurucz, R. L. *ATLAS9 Stellar Atmospheres Programs and 2 km s⁻¹ Grid*. (CD-ROM, Smithsonian Astrophysical Observatory, Cambridge, 1993).
- Kurucz, R. L., Furenlid, I., Brault, J., & Testerman, L. 1984, *Solar Flux Atlas from 296 to 1300 nm*, NOAO Atlas 1 (Cambridge: Harvard Univ. Press)
- Lai, D., Chernoff, D. F., & Cordes, J. M. 2001, *ApJ*, 549, 1111
- MacFadyen, A. I., Woosley, S. E., & Heger, A. 2001, *ApJ*, 550, 410
- Maeda, K., Nakamura, T., Nomoto, K., Mazzali, P. A., Patat, F., & Hachisu, I. 2002, *ApJ*, 565, 405
- Marsh, T. R., Robinson, E. L., & Wood, J. H. 1994, *MNRAS*, 266, 137
- Mignard, F. 2000, *A&A*, 354, 522
- Miller-Jones, J. C. A., Jonker, P. G., Nelemans, G., Portegies Zwart, S., Dhawan, V., Briskin, W., Gallo, E., & Rupen, M. P. 2009a, *MNRAS*, 394, 1440
- Miller-Jones, J. C. A., Jonker, P. G., Dhawan, V., Briskin, W., Rupen, M. P., Nelemans, G., & Gallo, E. 2009b, *ApJ*, 706, L230
- Mirabel, I. F., Dhawan, V., Mignani, R. P., Rodrigues, I., & Guglielmetti, F. 2001, *Nature*, 413, 139
- Mirabel, I. F., Mignani, R., Rodrigues, I., Combi, J. A., Rodríguez, L. F., & Guglielmetti, F. 2002, *A&A*, 395, 595
- Neilsen, J., Steeghs, D., & Vrtilik, S. D. 2008, *MNRAS*, 384, 849
- Orosz, J. A., et al. 2001, *ApJ*, 555, 489
- Orosz, J. A., & Baily, C. D. 1997, *ApJ*, 477, 876
- Pavlenko, E. P., Martin, A. C., Casares, J., Charles, P. A., & Ketsaris, N. A. 1996, *MNRAS*, 281, 1094
- Piskunov, N. E., Kupka, F., Ryabchikova, T. A., Weiss, W. W., & Jeffery, C. S. 1995, *A&AS*, 112, 525
- Podsiadlowski, P., Nomoto, K., Maeda, K., Nakamura, T., Mazzali, P., & Schmidt, B. 2002, *ApJ*, 567, 491
- Portegies Zwart, S. F., Verbunt, F., & Ergma, E. 1997a, *A&A*, 321, 207
- Portegies Zwart, S. F., Kouwenhoven, M. L. A., & Reynolds, A. P. 1997b, *A&A*, 328, L33
- Sanwal, D., Robinson, E. L., Zhang, E., Colome, C., Harvey, P. M., Ramseyer, T. F., Hellier, C., & Wood, J. H. 1996, *ApJ*, 460, 437
- Sadakane, K., et al. 2006, *PASJ*, 58, 595
- Shahbaz, T., Ringwald, F. A., Bunn, J. C., Naylor, T., Charles, P. A., & Casares, J. 1994, *MNRAS*, 271, L10

- Shahbaz, T., van der Hooft, F., Casares, J., Charles, P. A., & van Paradijs, J. 1999, MNRAS, 306, 89
- Shahbaz, T. 2003, MNRAS, 339, 1031
- Snedden, C. 1973, PhD Dissertation, Univ. of Texas at Austin
- Tominaga, N., Umeda, H. & Nomoto, K. 2007, ApJ, 660, 516
- Torres, M. A. P., Casares, J., Martínez-Pais, I. G., & Charles, P. A. 2002, MNRAS, 334, 233
- Torres, M. A. P., Callanan, P. J., Garcia, M. R., Zhao, P., Laycock, S., & Kong, A. K. H. 2004, ApJ, 612, 1026
- Umeda, H., & Nomoto, K. 2002, ApJ, 565, 385
- Umeda, H., & Nomoto, K. 2005, ApJ, 619, 427
- van Belle, G. T., et al. 1999, AJ, 117, 521
- van den Heuvel, E. P. J., & Habets, G. M. H. J. 1984, Nature, 309, 598
- van der Hooft, F., Heemskerk, M. H. M., Alberts, F., & van Paradijs, J. 1998, A&A, 329, 538
- Vogt, S. S., et al. 1994, Proc. SPIE, 2198, 362
- Zhao, G., Butler, K., & Gehren, T. 1998, A&A, 333, 219
- Zhao, G., & Gehren, T. 2000, A&A, 362, 1077